ACS SENSORS

pubs.acs.org/acssensors Article

Ultrasensitive and Reusable Graphene Oxide-Modified Double-Interdigitated Capacitive (DIDC) Sensing Chip for Detecting SARS-CoV-2

Parshant Kumar Sharma, Eun-Seong Kim, Sachin Mishra, Enkhzaya Ganbold, Ryun-Sang Seong, Ajeet Kumar Kaushik,* and Nam-Young Kim*

Cite This: *ACS Sens.* 2021, 6, 3468−3476 Read Online

ACCESS | Metrics & More | Article Recommendations | Supporting Information

ABSTRACT: This research reveals the promising functionalization of graphene oxide (GrO)-glazed double-interdigitated capacitive (DIDC) biosensing platform to detect severe acute respiratory syndrome coronavirus (SARS-CoV-2) spike (S1) proteins with enhanced selectivity and rapid response. The DIDC bioactive surface consisting of Pt/Ti featured SiO_2 substrate was fabricated using GrO/EDC-NHS/anti-SARS-CoV-2 antibodies (Abs) which is having layer-by-layer interface self-assembly chemistry method. This electroactive immune-sensing platform exhibits reproducibility and sensitivity with reference to the S1 protein of SARS-CoV-2. The outcomes of analytical studies confirm that GrO provided a desired engineered surface for Abs immobilization and amplified capacitance to achieve a wide detection range (1.0 mg/mL to 1.0 fg/mL), low limit of detection (1 fg/mL) within 3 s of response time, good linearity (18.56 nF/g), and a high sensitivity of 1.0 fg/mL. Importantly, the unique biochip was selective against blood-borne antigens and standby for 10 days at 5 °C. Our developed DIDC-based SARS-CoV-2 biosensor is suitable for point-of-care (POC) diagnostic applications due to portability and scaling-up ability. In addition, this sensing platform can be modified for the early diagnosis of severe viral infections using real samples.

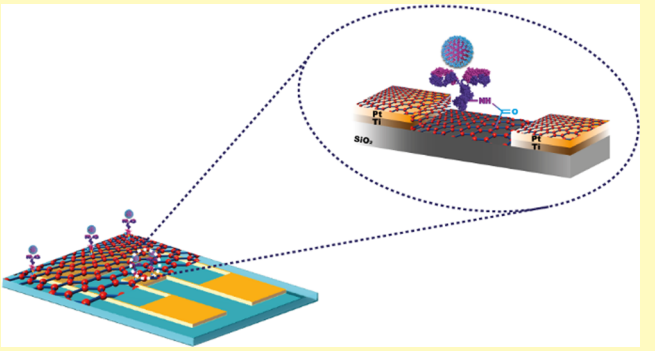

KEYWORDS: *SARS-CoV-2 spike (S1) protein, biochip, coronavirus, double-interdigitated capacitive biosensor, point-of-care, high sensitivity and good linearity, diagnostic applications*

The recent viral pandemic (COVID-19) associated with newly investigated β coronavirus,[1] i.e., severe acute respiratory syndrome coronavirus 2 (SARS-CoV-2),[2] caused a severe life-threatening global health emergency via affecting respiratory systems.[3] Due to its rapid human-to-human activity with high infectivity, mortality, and severe life-threatening adverse health effects,[4,5] virology research[6] evolved significantly faster to identify the SARS-CoV-2 structure, genome, and organization.[7,8] The COVID-19 symptoms include dry cough, high fever, and generalized pain.[9,10] Importantly, coinfection with different serotypes of SARS-CoV-2 usually leads to increased disease severity.[11] Additionally, asymptomatic carriers, with the potential to spread the virus, were identified. Under the microscope, these virus particles show clublike projections formed by the spike i.e., S1 proteins.[12] Therefore, to control the transmission and infectivity of COVID 19, the detection of SARS-CoV-2 must be timely and efficient. Thus, the selective, sensitive, and rapid detection of SARS-CoV-2 became essential to detect SARS-CoV-2 rapidly and selectively at the early stage of viral infection.[2,13] Health agencies highlighted the need for social/physical distancing to avoid the transmission of SARS-CoV-2, and expressed the importance of the development of smart diagnosis systems for targeted and mass testing.[14]

In practice, the real-time reverse-transcription polymerase chain reaction (RT-PCR) is the best way to detect SARS-CoV-2 similar to Middle-East respiratory syndrome coronavirus (MERS-CoV)[15] and SARS-CoV-1.[8] In this direction, the existing standard diagnosis of SARS-CoV-2 infection relies on the amplification of virus-specific sequences.[16,17] Considering the variability of SARS-CoV-2 infection concerning the region, population, race, and gender, it is essential to develop the rapid diagnosis tools for point-of-care (POC) application[18,19] with the final goal of saving lives.[13]

Received: July 6, 2021
Accepted: August 18, 2021
Published: September 3, 2021

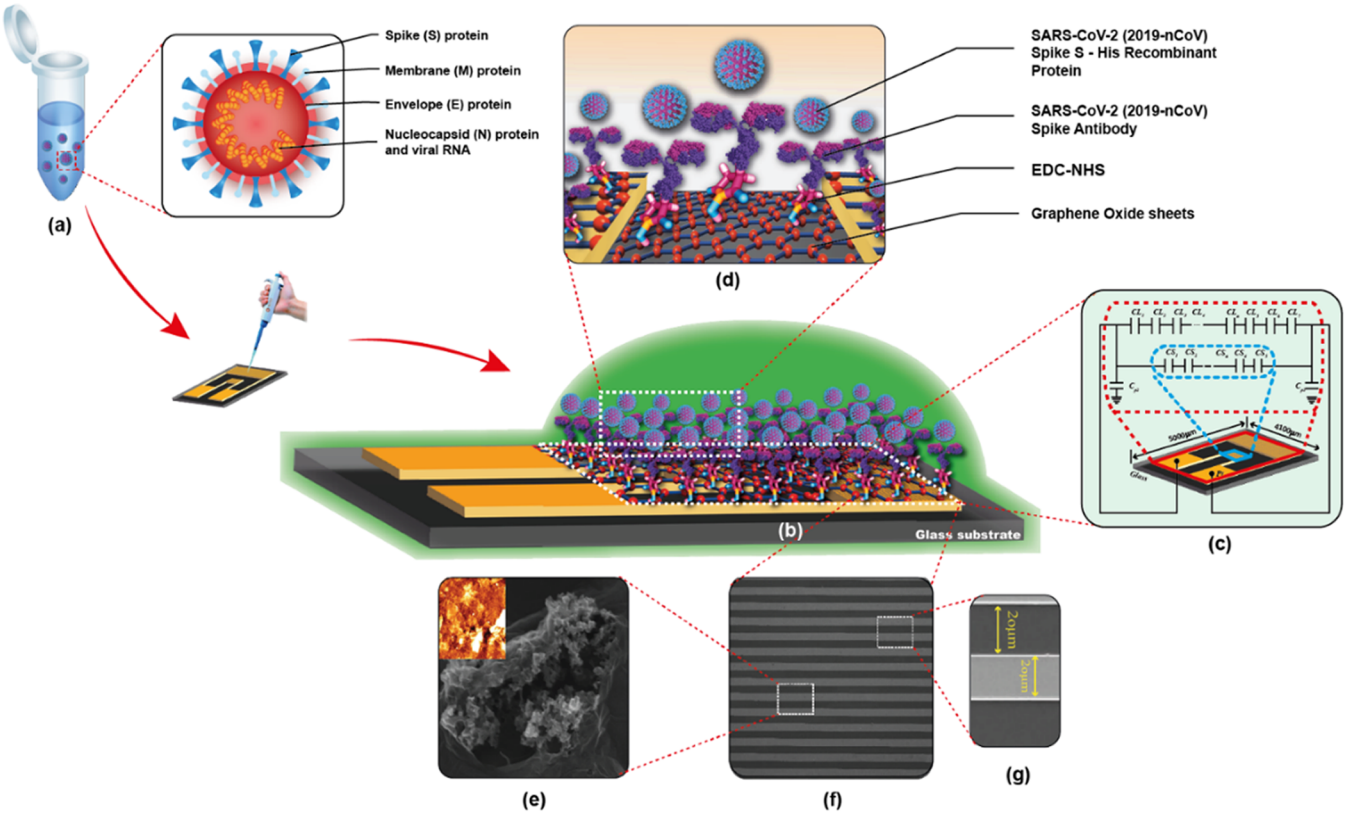

Figure 1. Schematic representation of the ultrasensitive and reusable graphene oxide-modified double-interdigitated capacitive (DIDC) sensing chip: (a) SARS-CoV-2 S-1 protein: SARS-CoV-2 structure with S1 protein; (b) layout setup of fabricated double-interdigitated capacitive (DIDC) sensing chip; (c) fabricated double-interdigitated capacitor (DIDC) with the equivalent circuit; CL: capacitor for large electrodes connected in series connection; and CS: capacitor for small central electrodes connected in series, the chip size is 4100 μm in width and 5000 μm in length; (d) GrO-modified double-interdigitated capacitive (DIDC) sensing chip with immobilized anti-SARS-CoV-2 Abs binding with SARS-CoV-2 S1 protein (targeted analyte); (e) morphology of anti-SARS-CoV-2 Abs embedded in GrO at 1 μm scale, inset image refers to atomic force microscopy (AFM) of GrO flakes equally distributed to the height of 25 nm; (f) SEM image of a bare chip; and (g) measurement of metal fingers, i.e., 20 μm and inter-distance between two metal fingers is defined.

In this direction, fluorescence in situ hybridization (FISH) assay, enzyme-linked immunosorbent assay (ELISA), electrochemical assay, and microsphere-based assays, magnetic resonance imaging (MRI) assay, positron emission tomography (PET), and ar-infrared fuorescenceocular imaging (NIRFOI)[20] are associated with low sensitivity, selectivity, and reusability along with such techniques also having drawbacks like expensive devices and specialized non-reusable reagents, as well as highly trained expertise personnel.[21] Consequently, analytical methods cannot be considered rapid, inexpensive, highly specific, and sensitive POC platforms.[22−24] There are a few DNA and antibody-based biosensors using chemical, electrical, and capacitive methods[16,17] for efficient diagnostics application. For instance, electrical DNA biosensors, associated with high sensitivity, easy miniaturization, and tunable features were developed for detecting Ebola,[25−27] Zika, MERS-CoV, and SARS-CoV.[28,29] On the same track, a field-effect transistor (FET)-based biosensor to detect SARS-CoV-2 S1 protein using specific monoclonal antibodies (Abs) immobilized onto a graphene channel was successfully fabricated.[30−32] However, the above methods of SARS-CoV-2 detection was less sensitive than RT-PCR. Recently, an Aerosol Jet nanoparticle reduced graphene oxide (GrO)-coated three-dimensional (3D) electrode-based sensing system for SARS-CoV-2 with a low detection limit (2.8×10^{-15} M) was also developed. In spite of outstanding sensing parameters, the proposed sophisticated biosensor structure[30] may be challenging to perform POC diagnosis applications.

To overcome the abovementioned limitations, this research signifies development of a miniaturized and reusable GrO-modified double-interdigitated capacitive (DIDC) biosensor for detecting SARS-CoV-2 S1 protein at femtogram (fg) level within 3 s. To detect low concentration of SARS-CoV-2 protein (can be taken out from oropharyngeal or nasopharyngeal swabs), GrO nanoflakes were selected to achieve the desired sensitivity and selectivity. GrO is an unsubstantial, chemically reliable, steady, and conductive material that can be productively used for biosensing applications;[2,33,34] for selectivity, we utilized monoclonal IgG Abs, a label-free hybridization approach to target SARS-CoV-2 S1 protein. Importantly, our fabricated SARS-CoV-2-GrO-DIDC biosensor is reusable after optimized ozone treatment and piranha cleaning. Overall, this ultrafast, affordable, label-free, ultrasensitive, and reusable biosensor has the potential to perform well in the context of clinical and POC applications.

FUNCTIONALIZATION AND DETECTION OF SARS-COV-2 SPIKE (S1) PROTEIN

Design of DIDC Electrodes. For making an efficient DIDC-based biosensor, dielectric constant, charge distribution, and conductivity of DIDC were observed to be of high significance. Importantly, the changes in these sensing

https://doi.org/10.1021/acssensors.1c01437
ACS Sens. 2021, 6, 3468−3476

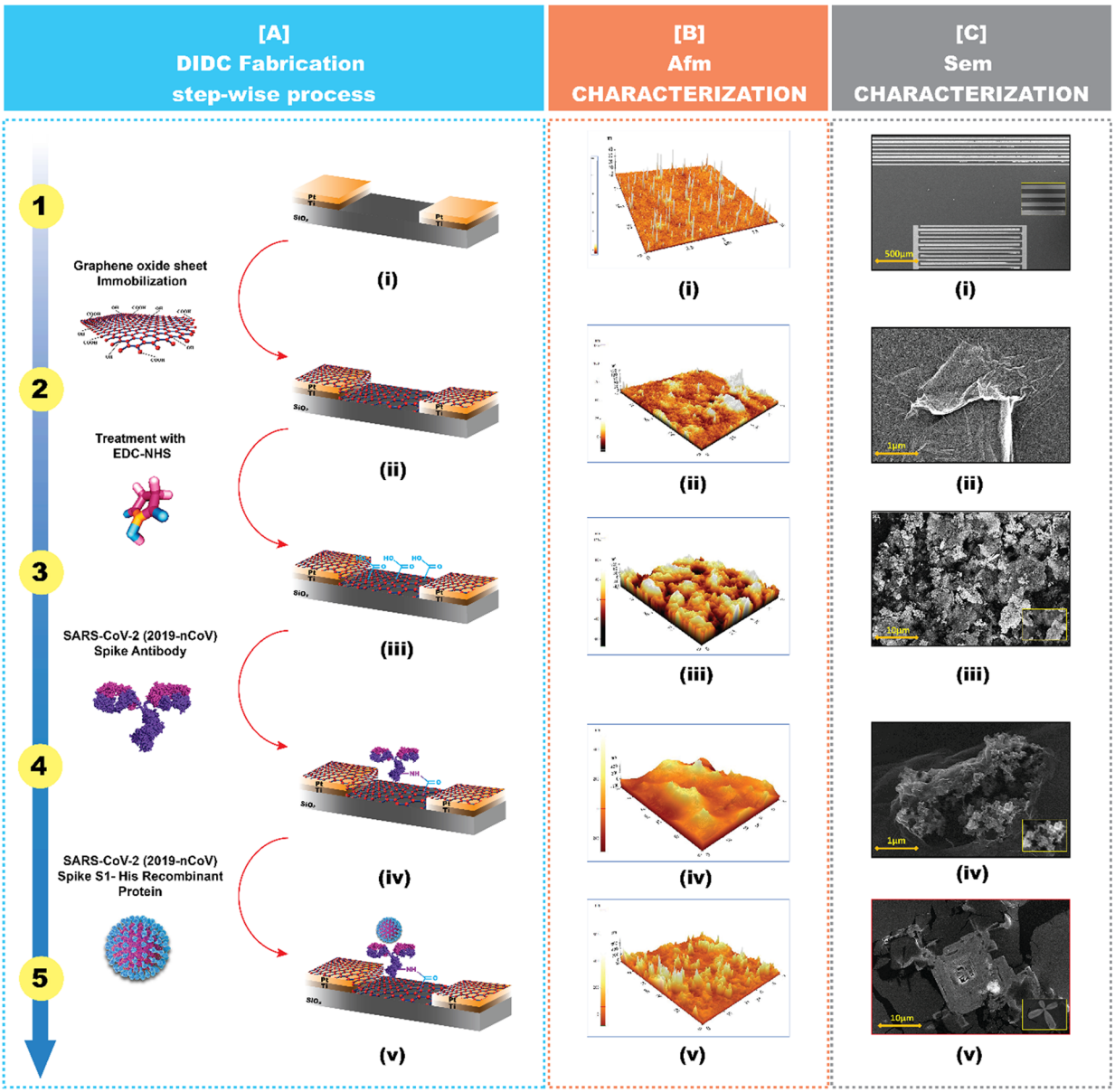

Figure 2. DIDC fabrication stepwise process and evaluation of surface changes and functionalities via atomic force microscopy (AFM) and scanning electron microscopy (SEM): (A) fabricated DIDC sensing chip: layout with the sequential circuit (Figure 1c) of modifications: (i) effective photoresist-coated Eagle XG SiO_2 wafer Pt/Ti electrode bare DIDC chip, (ii) DIDC chip, coated by GrO at 1300 rpm, (iii) EDC-NHS coupling for GrO-glazed DIDC chip, (iv) immobilization of anti-SARS-CoV-2 S1 antibodies via EDC-NHS coupling (EDC-NHS-GrO-Pt/Ti-SiO_2)DIDCs via "*tail-on*" Ab-specific orientation, and (v) SARS-CoV-2 S1 protein binding on SARS-CoV-2-Ab-EDC-NHS-GrO-Pt/Ti-SiO_2)DIDCs. (B) AFM characterization for surface morphology: high-resolution images of the DIDC chip surfaces: (i) DIDC bare chip, (ii) GrO-functionalized chip, (iii) EDC-NHS chemistry activated chip, (iv) anti-SARS-CoV-2 Abs immobilization, and (v) SARS-CoV-2 S1 protein. (C) SEM surface morphology: (i) DIDC bare chip at 500 μm, (ii) GrO flakes at 1 μm, (iii) EDC-NHS coupling image at 10 μm, (iv) anti-SARS-CoV-2 Abs embedded in GrO at 1 μm, and (v) SARS-CoV-2(2019-nCoV) S1 protein as robust covalent "*tail-on*" Ab-specific orientation at 10 μm.

parameters correspond to the capacitive reactance of the DIDC.[16,31,35] In this research, we envisioned a capacitance immunosensor composed of anti-SARS-CoV-2 Abs functionalized via 1-ethyl-3-(3-dimethylaminopropyl)carbodiimide−*N*-hydroxy succinimide (EDC-NHS) coupling on the GrO-DIDC-based SiO_2 substrate.[30] In this process, EDC-NHS (cross-linker) was attached via covalent bonds onto the GrO substrate for the functionalization of anti-SARS-CoV-2 Abs. The schematic of our proposed biosensor is represented in Figure 1.

FABRICATION OF DIDC-BASED SARS-COV-2 BIOSENSOR

The fabrication of SARS-CoV-2 S1 protein-DIDC biosensor detection is positioned on three key factors, i.e., charge distribution, dielectric constant, and conductivity.[16,35,36] When the analytes is placed onto DIDC biosensor, the dielectric constant, charge distribution, and conductivity with the antibody and antigen are altered in terms of sensing parameters corresponding to the capacitive reactance of the DIDC voltage. A schematic representation of the conducted research workflow is depicted in Figure 2A(i−v).

https://doi.org/10.1021/acssensors.1c01437
ACS Sens. 2021, 6, 3468−3476

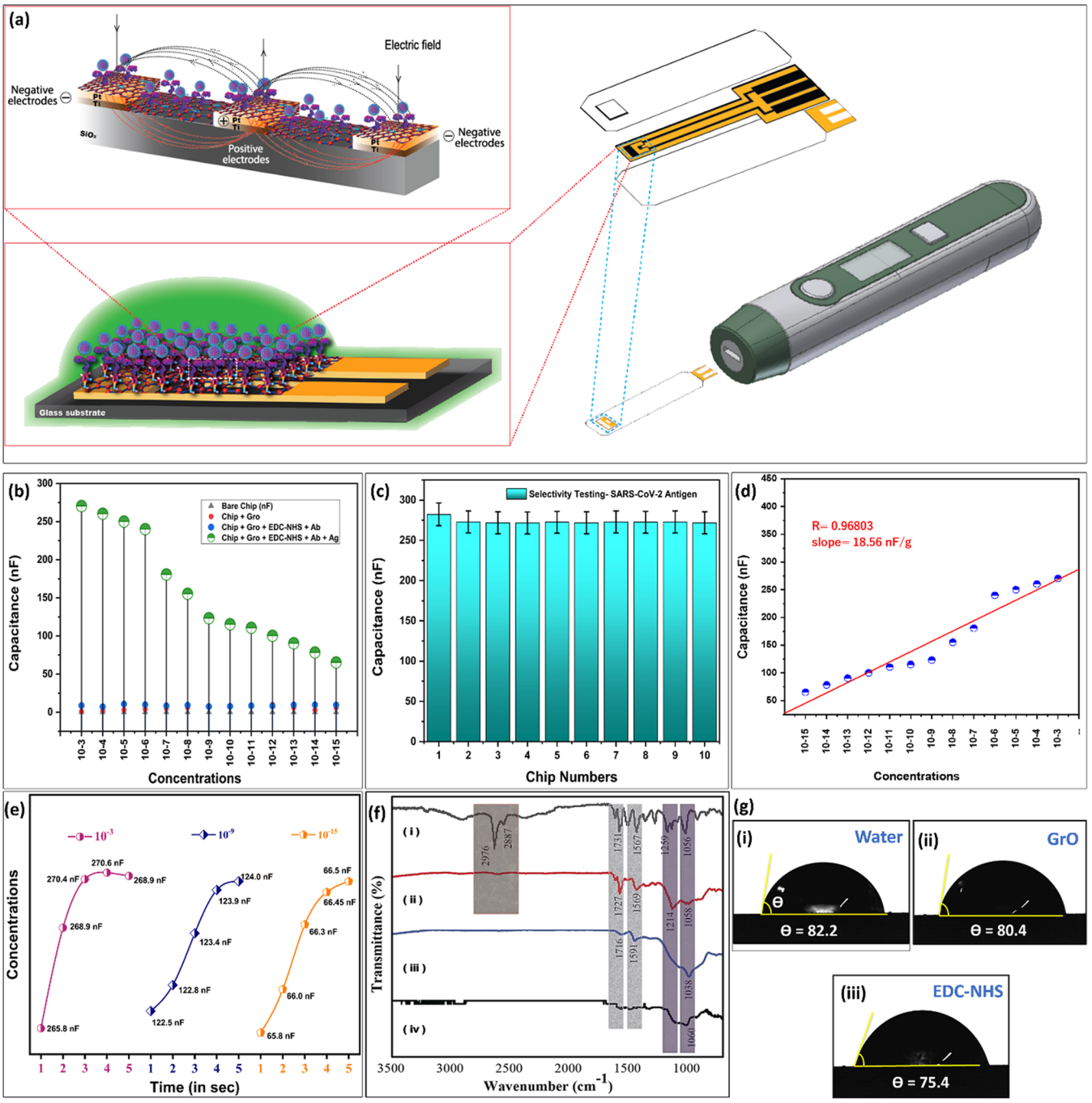

Figure 3. (a) Pt/Ti-based DIDC electrodes bound by SARS-CoV-2 Abs and SARS-CoV-2 biomolecules disrupting the electric field between the metal electrodes (metal fingers), capacitive coupling effect, and the fabricated DIDC chip with capacitance measurement device. (b) Sensitivity of the prepared SARS-CoV-2-Ab-EDC-NHS-GrO-Pt/Ti-SiO_2)DIDCs immunoplatform sensing chip for 1.0 mg/mL to 1.0 fg/mL wide range detection, capacitance values of bare chip, Chip-GrO, Chip-Gro-EDC-NHS−SARS-CoV-2-Ab, and Chip-GrO-EDC-NHS−SARS-CoV-2-Ab-SARS-CoV-2-Ag (1.0 mg/mL to 1.0 fg/mL). (c) Selectivity of the prepared SARS-CoV-2-Ab-EDC-NHS-GrO-Pt/Ti-SiO_2 DIDCs immunoplatform biosensor in the presence and absence of interfering protein. (d) Good linearity, i.e., 18.56 nF/g for a wide range of detection (1.0 mg/mL to 1.0 fg/mL), indicating the worthy linear regression line (solid); the slope and regression coefficient (R) value are calculated by fitting the data. (e) Response times of 1×10^{-3}, 1×10^{-9}, and 1.0×10^{-15} g/mL concentration with stable capacitance value (within 3 s); (f) FTIR spectroscopic characterization: (i) anti-SARS-CoV-2 antibodies, (ii) EDC-NHS coupling, (iii) DIDC chip glazed with graphene oxide, and (iv) bare DIDC chip; and (g) wettability measurements: (i) bare DIDC chip (82.0 ± 3°), (ii) graphene oxide (80.4 ± 3°), and (iii) EDC-NHS (75.4 ± 3°).

The DIDC is evaluated using a LCR meter (hand held, 1 kHz, 2 kH, 200 pF, 0.2 Gohm, U1730C Series) with a PC for data acquisition as shown in Figure 2A(i). The measurement was obtained at 0 V direct current (DC) bias voltage with a 1-kHz frequency across the DIDC biosensor. First, the sensor domain was triggered with the piranha solution at a 3:1 ratio (H_2SO_4:H_2O_2) at 80 °C and then rinsed with deionized (DI) water to remove the reagents resulting in a hydrophilic surface as reported elsewhere.[37,38] After the activation process, the surface was coated with GrO (4 μL) at 1300 rpm via spin

https://doi.org/10.1021/acssensors.1c01437
ACS Sens. 2021, 6, 3468−3476

coating method (Figure 2A(ii)). Then, GrO onto the DIDC chip was annealed on a hot plate at 80 °C for 1 h. After the annealing process, EDC-NHS (4 μL; 0.4 and 0.1 M, respectively) chemistry was performed[39] using an optimized process to generate the covalent conjugation of amine and carboxylic groups via amide bond formation represented in Figure 2A(iii). Next, a reconstitution buffer was prepared with 0.1 M reactant buffer and 1 μg/mL purified antibody. For the conjugation of SARS-CoV-2 Abs (reproduced by Rabbit mAbs anti-S1 protein), a drop (4 μL) was cast onto the NHS-activated GrO (Figure 2A(iv)). Of note, the Fab region of Abs usually contains abundant reactive amine and carboxylic groups due to its polar nature; therefore, the successive specific immobilization results in robust covalent "*tail-on*" Ab-specific orientation as defined in Figure 2A(v).[40] Importantly, treatment with bovine serum albumin (BSA) was used to block the nonspecific sites of the sensor under agitation, at room temperature for 20 min in a closed container. After drying, capacitive immunosensor was placed in a closed container immediately before use. The DIDC-based capacitive immunosensor (SARS-CoV-2-Ab-EDC-NHS-GrO-Pt/Ti-SiO_2-DIDCs) is now ready to be used for the serial detection of the SARS-CoV-2 S1 protein. All of the testing were performed in a contamination-free chamber and the moisture, other matrix parameters were controlled.

EVALUATION OF TOPOLOGICAL SURFACE CHANGES AND BIOFUNCTIONALIZATION

Surface characterization of the DIDC chip, alone, or in the context of GrO, EDC-NHS, anti-SARS-CoV-2 S1 Abs, and SARS-CoV-2 S1 protein was performed via atomic force microscopy (AFM) and scanning electron microscopy (SEM).

The process of surface functionalization is classified as shown in Figure 2B(i−v). The five consecutive surfaces showed different morphologies and heights in microscale levels. The bare chip surface morphology is shown in Figure 2B(i) up to 5 nm. A homogeneous morphology of GrO was observed on the DIDC chip up to 25 nm (Figure 2B(ii)), while the EDC-NHS cross-linker was distributed onto the GrO-functionalized DIDC chip at a height of 40 nm (Figure 2B(iii)). As expected, an additional increase in the height was observed after immobilization of anti-SARS-CoV-2 antibodies onto the EDC-NHS-GrO-Pt/Ti DIDC chip, up to 400 nm (Figure 2B(iv)), confirming that the anti-SARS-CoV-2 antibodies were immobilized into the functionalized DIDC chip. Moreover, after the addition of the SARS-CoV-2 S1 protein, a sharp peak has been observed up to the height of 600 nm due to the presence of the S1 protein, as shown in Figure 2B(v), which indicated the antibody−antigen "*tail-on*" binding orientation (Figure S1a−d).

The typical top-view SEM images are shown in Figure 2C(i−v). Figure 2C(i) at 500 μm presented the effective photoresist-coated Eagle XG SiO_2 wafer onto Pt/Ti electrode bare DIDC chip; inset: the measurement of between two metal fingers, i.e., 20 μm. The DIDC-coated samples showed a smoother and more homogeneous surface morphology; the GrO-functionalized, EDC-NHS-activated, anti-SARS-CoV-2 antibody-functionalized, and SARS-CoV-2 S1 protein chips are shown in panels (ii), (iii), (iv), and (v), respectively. The exfoliated graphene oxide flakes furnish the desired functionality with hydroxyl groups (−OH) and carboxylic groups (−COOH), which enhanced the sensing performance in terms of sensitivity and selectivity. Figure 2C(ii) shows the homogeneous GrO flakes distribution at 1 μm. Figure 2C(iii) shows the EDC-NHS coupling and a hollow cylindrical structure for anti-SARS-CoV-2 antibody binding at 3 μm. Figure 2C(iv) shows the antibodies embedded in GrO-EDC-NHS functionalized sensing chip at 1 μm. Figure 2C(v) shows the SARS-CoV-2 protein like a pool structure bonded with antibody at 10 μm (Figure S2a−d). The formation of new expected bonds during stepwise fabrication of the GrO-DIDC biosensor was characterized using Fourier transform infrared (FTIR) spectroscopy, as shown in Figure 3f(i−iv). The results of FTIR spectroscopy are as follows: (i) a C−H stretching peak at 2976 cm^{-1} defined the presence of antibodies on the chip surface, (ii) an N−O sharp peaking at 1569 cm^{-1} highlighting the presence of nitro groups after EDC-NHS functionalization, (iii) a peak at 1038 cm^{-1} referring to C−O bonds (aromatic ester), suggesting the presence of aromatic rings in the context of GrO immobilized onto the biochip, and (iv) bare biochip showing the C−O primary alcohol with weak intensities peaking at 1060 cm^{-1}.

Additionally, the wettability of the different chips was measured in the context of the observation of the contact angle (θ) of a 5 μL water drop. The water exhibited a higher contact angle (around 82.0 ± 3°) in the context of bare chips (Figure 3g(i)). Of note, this angle decreased in the presence of GrO (80.4 ± 3°) (Figure 3g(ii)), and EDC-NHS (75.4 ± 3°) (Figure 3g(iii)). Altogether, these contact angles (θ) indicate that GrO and EDC-NHS-treated chips are more hydrophilic than the bare DIDC electrode.

RESULTS AND DISCUSSION

Assessment of Sensitivity, Selectivity, and Response Time. The proposed reusable DIDC immunosensor bionic chip was designed and fabricated for the determination of the SARS-CoV-2 protein via immobilization of specific monoclonal antibodies onto a GrO-EDC-NHS functionalized SiO_2-Pt/Ti. It was also used as a biocompatible material and template for the conjugation of anti-SARS-CoV-2 Abs, thereby demonstrating the ability of the cross-linkers to enhance the charge transfer rate to verify the impact in terms of electrical capacitance value (Figure 3a). Remarkably, the immunosensor demonstrated a limit of detection (LOD) value of 1.0 fg/mL, lower than the existing countless biosensors for the detection of SARS-CoV-2. Importantly, the proposed electrical capacitive immunosensor also performs better as compared with other electrochemical affinity biosensors described so far for the detection of SARS-CoV-2 protein, in terms of sensitivity, selectivity, reusability, and response time.

To test the sensitivity of the developed SARS-CoV-2-Ab-EDC-NHS-GrO-Pt/Ti-SiO_2 DIDC immunoplatform, we selected successive different concentrations of the SARS-CoV-2 S1-His protein (ranging from 1.0×10^{-3} to 1.0×10^{-15} g) using the drop-casting method onto the DIDC chips to measure the capacitance in the context of different protein/antigen concentrations, and the spectra were compared with those of control conditions (Figure 3b).

Additionally, we also measured the selectivity of SARS-CoV-2 protein (Figure 3c), in the context of potentially interfering compounds coexisting in biological samples, such as prostate-specific antigen (PSA) and amyloid β_{1-42} act as a interfering protein. The concentration of interfering protein is 1.0 μg/mL for both PSA and amyloid β_{1-42}. The selectivity test was performed in the presence and absence of interfering proteins. Testing has been performed with 10 different DIDC sensors,

https://doi.org/10.1021/acssensors.1c01437
ACS Sens. 2021, 6, 3468−3476

from sensors 1−5 tested in the presence of the interfering protein and the rest DIDC sensors 6th−10th sensors tested in the absence of the interfering protein. There were no such capacitance changes observed. From sensors 1−5, the capacitance varied from 286.9 to 275.5 nF and from sensors 6−10 the capacitance value varied from 271.9 to 273 nF maximum to minimum values, respectively. All of the samples were diluted in 0.1 M × phosphate-buffered saline (PBS) solution (pH 7.4). The tests were performed via the measurement of 1.0 μg/mL SARS-CoV-2 S1 protein samples in the absence and presence of the nontarget protein biomolecules. This immunoplatform could provide quantitative results in the context of 5 μL samples in seconds, after a single incubation step; the capacitance changed in 3 s in the context of SARS-CoV-2 protein, with no significant cross-reactivity with nonspecific analytes. The sensitivity measurement of the SARS-CoV-2 protein is mentioned via capacitance vs concentrations relation by the equation of a straight line, i.e., $y = mx + c$. Here, y is a function of x, m is the gradient angle of the line to x-axis, and c is the intercept on the y-axis. In statistical calculation, every measurement was performed a minimum three times and an average value was used; the sensitivity was defined as 18.56 nF/g (Figure 3d). To check the response time of the developed SARS-CoV-2-Ab-EDC-NHS-GrO-Pt/Ti-SiO_2-DIDC immunoplatform, we have selected three different antigen concentrations, i.e., 1×10^{-3}, 1×10^{-9}, and 1.0×10^{-15} g/mL. The capacitance value become stabilized within 3 s at the level of each concentration as presented in Figure 3e. The DIDC capacitance is one of the fastest detection methods that has been reported till date. Therefore, altogether, our results support the usefulness of our biosensor in the clinical context (Tables S1 and S2).

Evaluation of Stability, Reproducibility, and Reusability. Next, the stability of the biocomposite[41] SARS-CoV-2-Ab-EDC-NHS-GrO-Pt/Ti-SiO_2 DIDCs was analyzed; chips were stored at 5 °C in a humid chamber for 10 days. Importantly, no significant changes were observed in the performance of the biochip with the increase of the storage time (Figure S3i).

Additionally, the reproducibility of our fabricated DIDC-based sensor for SARS-CoV-2 detection was also evaluated (Figure S3ii). Concerning the reproducibility, the capacitance values in the context of SARS-CoV-2-Ab-EDC-NHS-GrO-Pt/Ti-SiO_2-DIDCs were measured for 10 h. Importantly, the capacitance values were stable, with no more than ±5% deviation in the context of pillar-to-pillar values. Additionally, in line with the stability results above, we also assessed the reproducibility results in time, for 10 days. Of note, these capacitance values also showed a variation lower than ±5% in the context of pillar-to-pillar values. Of note, on the 2nd day, we observed a little difference (from 8.8 to 7.2 nF), probably due to the transfer of the chip from room temperature to low temperature; however, from day 2 onward, the capacitance values were stable. Importantly, from day 1 to day 10, the capacitance values varied from 8.8 to 7.2 nF, with no significant changes observed in repeatability/reproducibility with mean ($\bar{x}$), standard deviation (SD), and relative standard deviation (RSD) values as shown in Table S3.

Finally, we also evaluated the reusability potential of the SARS-CoV-2 DIDC biochip. To elute the antibodies from the sensor surface, we used glycine-HCl elution buffer (0.1 M) with a low pH (2.7); of note, we chose a pH outside of the physiological range (7−7.4) of the body pH to ensure the disruption of immunoaffinity. Importantly, the introduction of the elution buffer for 1 min onto the sensor led to the capacitance signal to levels like those in the context of the functionalized GrO (1.2 nF). Afterward, the DIDC sensor was further exposed to piranha solution at 80 °C, and then the capacitance was measured with levels nearly equal to that of the bare DIDC chip (0.026 nF); the DIDC chip was recovered to 96% of its bare values. Of note, the results were similar after the 1st and 2nd regeneration, with no significant changes, as presented in Figures S4i,ii and S5.

The carefully designed protocol for the sensor surface preparation, anti-SARS-CoV-2 Abs immobilization, and hybridization with SARS-CoV-2 S1 protein strike a balance among the competing factors of ease of immobilization, specificity, and the overall capacitance measurement quality. The development of GrO-modified DIDC biochip was verified using electrical and optical surface analyses. Noteworthily, the large surface area of graphene-based materials facilitates the adsorption of different analytes. Additionally, the reusability of our GrO-DIDC ultrasensitive and rapid sensor biochip demonstrates an easy and acceptable procedure for POC testing. Therefore, the reported biosensor improves the state-of-the-art as per the three overlooks. First, the sensor was able to produce an output of more than 70 nF in capacitance change in response to the bare DIDC chip glazed with GrO at a lowest concentration of 1.0 fg/mL. The magnitude of capacitance change increases linearly with the target SARS-CoV-2 protein concentrations in the range between 1.0 mg/mL and 1.0 fg/mL. The detection limit of our biosensor is among the lowest reported till date for a non-faradic capacitive biosensor. Second, sensor specificity is exhibited by the change in the way of capacitance differential between target and nontarget protein. For the nontarget protein, the measured change in the capacitance is significantly less than the target SARS-CoV-2 protein target protein, and it does not display an appreciable change in the capacitance as the nontarget molecule concentration increases. Third, the sensor achieved a dynamic range for the detection between 1.0 mg/mL and 1.0 fg/mL with excellent linearity of 18.56 nF/g in capacitance changes. On the one hand, the rapid SARS-CoV-2 S1 protein detection allows rapid tracking of primary contacts, extends the therapeutic window of opportunity, and supports the targeted treatment; on the other hand, it facilitates the spread of a disease, which helps to get the pandemic under control in a short period.

Particularly, this inexpensive biosensor enabling the accurate detection of very low concentrations of SARS-CoV-2 S1 protein can have drastic implications in the confinement and management of the current viral pandemic. Of note, the combination of graphene-based biosensors working along with smartphones is of great promise for the development of low-cost, reliable, and versatile (bio)sensing platforms, which can be widely applied on-site, i.e., as POC devices. These features, combined with high sensitivity, selectivity, and large-scale production potential, support the broad applicability of graphene-based sensors for the detection of various viral agents.

CONCLUSIONS AND VIEWPOINT

We have developed ultrasensitive and reusable graphene oxide-modified double-interdigitated capacitive (DIDC) sensing chip to detect SARS-CoV-2 S1 proteins with better selectivity at fg concentrations. Our research findings revealed that introducing

https://doi.org/10.1021/acssensors.1c01437
ACS Sens. 2021, 6, 3468−3476

GrO-functionalized DIDC capacitive sensor improves the binding strength that boosts the sensitivity and selectivity of the device. The narrow line shape and electrical property changes (impedance coupling) enabled the capacitance changes for a variety of unique detection ranges (1.0×10^{-3}–1.0×10^{-15} g). The performance of the DIDC capacitive sensor device was carefully probed in highly diluted solutions containing BSA biomolecules and the S1 protein. This set of studies proved that the proposed DIDC capacitive sensor can be utilized in the detection of SARS-CoV-2 S1 proteins in real assays with a fairly short sample-to-result duration (~5–6 s). We contemplate that the proposed noninvasive and rapid technique in this work allows for the diagnosis of SARS-CoV-2 S1 protein at very early stages with high accuracy.

In the future, we aim to detect SARS-CoV-2 proteins at POC that enables the patient-centric treatment and management after optimizing all of the device components, i.e., sensing chip (presented in this manuscript), full integration of prototype-based DIDC capacitive sensor with real patient samples (in the process), and ultimately interfacing of the analytical unit with a smart display system (in the process) and sensing COVID-19 using smartphone-based operation. However, the studied and presented sensor device is not yet tested using real samples due to a lack of administrative formalities. Serious efforts are being made to establish a collaboration between South Korean virology and Infection lab-based and overseas hospitals to arrange biofluids of COVID-19-infected patients. The results of the complete future studies related to POC diagnostics of COVID-19 using our high-performance capacitive sensor will be published elsewhere.

■ ASSOCIATED CONTENT

Supporting Information

The Supporting Information is available free of charge at https://pubs.acs.org/doi/10.1021/acssensors.1c01437.

This research reveals the promising functionalization of graphene oxide (GrO)-glazed double-interdigitated capacitive (DIDC) biosensing platform to detect severe acute respiratory syndrome coronavirus (SARS-CoV-2) spike (S1) protein (severe acute respiratory syndrome) selectively and rapidly; in this research, several chemicals and equipment; for the morphological analysis, scanning electron microscopy (SEM), atomic force microscopy (AFM), Fourier transform infrared spectroscopy (FTIR), and OCA 25 apparatus (Dataphysics Instruments) for the diffusivity and wettability of the sensing surfaces; LCR meter (Impedance analyzer) has been used to analyze the capacitance (1–100 kHz) of the different bionic electrodes; DIDC chip reusability factor; some important biosensors for the detection of CoVs; some important biosensing techniques used for SARS-CoV-2 detection and their properties; evaluation of repeatability/reproducibility with mean ($\bar{x}$), standard deviation (SD), and relative standard deviation (RSD) values (PDF)

■ AUTHOR INFORMATION

Corresponding Authors

Ajeet Kumar Kaushik − *NanoBioTech Laboratory, Health Systems Engineering, Department of Environmental Engineering, Florida Polytechnic University, Lakeland, Florida 33805, United States;* orcid.org/0000-0003-4206-1541; Email: akaushik@floridapoly.edu

Nam-Young Kim − *RFIC Bio Centre, Kwangwoon University, Seoul 01897, South Korea; Department of Electronics Engineering and NDAC Centre, Kwangwoon University, Seoul 01897, South Korea;* orcid.org/0000-0003-4264-2928; Email: nykim@kw.ac.kr

Authors

Parshant Kumar Sharma − *RFIC Bio Centre, Kwangwoon University, Seoul 01897, South Korea; Department of Electronics Engineering, Kwangwoon University, Seoul 01897, South Korea;* orcid.org/0000-0002-1328-2823

Eun-Seong Kim − *RFIC Bio Centre, Kwangwoon University, Seoul 01897, South Korea; Department of Electronics Engineering, Kwangwoon University, Seoul 01897, South Korea*

Sachin Mishra − *RFIC Bio Centre, Kwangwoon University, Seoul 01897, South Korea; Department of Electronics Engineering and NDAC Centre, Kwangwoon University, Seoul 01897, South Korea;* orcid.org/0000-0002-5132-9872

Enkhzaya Ganbold − *RFIC Bio Centre, Kwangwoon University, Seoul 01897, South Korea; Department of Electronics Engineering, Kwangwoon University, Seoul 01897, South Korea;* orcid.org/0000-0002-2195-7480

Ryun-Sang Seong − *RFIC Bio Centre, Kwangwoon University, Seoul 01897, South Korea; Department of Electronics Engineering, Kwangwoon University, Seoul 01897, South Korea*

Complete contact information is available at: https://pubs.acs.org/10.1021/acssensors.1c01437

Author Contributions

P.K.S.—investigation, validation, writing (original draft), visualization, software, and graphics designing; E.-S.K.—DIDC (double-interdigitated capacitive) chip designing; S.M.—formal analysis and software; E.G.—graphics designing; R.-S.S.—reference setting; A.K.K.—formal analysis, review & editing, and supervision; N.-Y.K.—supervision, project administration, funding acquisition, and resources.

Notes

The authors declare no competing financial interest.

All reagents used in this manuscript are available from commercial sources.

■ ACKNOWLEDGMENTS

This work was supported in part by the Basic Science Research Program through the National Research Foundation of Korea (NRF) funded by the Ministry of Education under Grants 2018R1A6A1A03025242 and 2018R1D1A1A09083353, and in part by the Korea Ministry of Environment (MOE) Graduate School specialized in Integrated Pollution Prevention and Control Project and a Research Grant of Kwangwoon University in 2020.

■ REFERENCES

(1) Boldog, P.; Tekeli, T.; Vizi, Z.; Dénes, A.; Bartha, F. A.; Röst, G. Risk Assessment of Novel Coronavirus COVID-19 Outbreaks Outside China. *J. Clin. Med.* **2020**, *9*, 571–583.

(2) Seo, G.; Lee, G.; Kim, M. J.; Baek, S.-H.; Choi, M.; Ku, K. B.; Lee, C.-S.; Jun, S.; Park, D.; Kim, H. G.; Kim, S.-J.; Lee, J.-O.; Kim, B. T.; Park, E. C.; Kim, S. I. Rapid detection of COVID-19 causative

virus (SARS-CoV-2) in human nasopharyngeal swab specimens using field-effect transistor-based biosensor. *ACS Nano* **2020**, *14*, 5135−5142.
(3) Panda, P. K.; Arul, M. N.; Patel, P.; Verma, S. K.; Luo, W.; Rubahn, H. G.; Mishra, Y. K.; Suar, M.; Ahuja, R. Structure-based drug designing and immunoinformatics approach for SARS-CoV-2. *Sci. Adv.* **2020**, *6*, eabb8097−eabb8111.
(4) Li, R.; Pei, S.; Chen, B.; Song, Y.; Zhang, T.; Yang, W.; Shaman, J. Substantial undocumented infection facilitates the rapid dissemination of novel coronavirus (SARS-CoV-2). *Science* **2020**, *368*, 489−493.
(5) Goel, S.; Hawi, S.; Goel, G.; Thakur, V. K.; Agrawal, A.; Hoskins, C.; Pearce, O.; Hussain, T.; Upadhyaya, H. M.; Cross, G.; Barber, A. H. Resilient and agile engineering solutions to address societal challenges such as coronavirus pandemic. *Mater. Today Chem.* **2020**, *17*, 100300−100323.
(6) Lu, R.; Zhao, X.; Li, J.; Niu, P.; Yang, B.; Wu, H.; Wang, W.; Song, H.; Huang, B.; Zhu, N.; Bi, Y.; Ma, X.; Zhan, F.; Wang, L.; Hu, T.; Zhou, H.; Hu, Z.; Zhou, W.; Zhao, L.; Chen, J.; Meng, Y.; Wang, J.; Lin, Y.; Yuan, J.; Xie, Z.; Ma, J.; Liu, W. J.; Wang, D.; Xu, W.; Holmes, E. C.; Gao, G. F.; Wu, G.; Chen, W.; Shi, W.; Tan, W. Genomic characterisation and epidemiology of 2019 novel coronavirus: implications for virus origins and receptor binding. *Lancet* **2020**, *395*, 565−574.
(7) Hui, D. S.; Azhar, E. I.; Madani, T. A.; Ntoumi, F.; Kock, R.; Dar, O.; Ippolito, G.; Mchugh, T. D.; Memish, Z. A.; Drosten, C.; Zumla, A.; Petersen, E. The continuing 2019-nCoV epidemic threat of novel coronaviruses to global health - The latest 2019 novel coronavirus outbreak in Wuhan, China. *Int. J. Infect. Dis.* **2020**, *91*, 264−266.
(8) Lu, X.; Whitaker, B.; Sakthivel, S. K. K.; Kamili, S.; Rose, L. E.; Lowe, L.; Mohareb, E.; Elassal, E. M.; Al-sanouri, T.; Haddadin, A.; Erdman, D. D. Real-Time Reverse Transcription-PCR Assay Panel for Middle East Respiratory Syndrome Coronavirus. *J. Clin. Microbiol.* **2014**, *52*, 67−75.
(9) Chen, I.-Y.; Chang, S. C.; Wu, H.-Y.; Yu, T.-C.; Wei, W.-C.; Lin, S.; Chien, C.-L.; Chang, M.-F. Upregulation of the Chemokine (C-C Motif) Ligand 2 via a Severe Acute Respiratory Syndrome Coronavirus Spike-ACE2 Signaling Pathway. *J. Virol.* **2010**, *84*, 7703−7712.
(10) Fung, T. S.; Huang, M.; Liu, D. X. Coronavirus-induced ER stress response and its involvement in regulation of coronavirus-host interactions. *Virus Res.* **2014**, *194*, 110−123.
(11) Fajnzylber, J.; Regan, J.; Coxen, K.; Corry, H.; Wong, C.; Rosenthal, A.; Worrall, D.; Giguel, F.; Piechocka-Trocha, A.; Atyeo, C.; Fischinger, S.; Chan, A.; Flaherty, K. T.; Hall, K.; Dougan, M.; Ryan, E. T.; Gillespie, E.; Chishti, R.; Li, Y.; Jilg, N.; Hanidziar, D.; Baron, R. M.; Baden, L.; Tsibris, A. M.; Armstrong, K. A.; Kuritzkes, D. R.; Alter, G.; Walker, B. D.; Yu, X.; Li, J. Z.; Abayneh, B. A.; Allen, P.; Antille, D.; Balazs, A.; Bals, J.; Barbash, M.; Bartsch, Y.; Boucau, J.; Boyce, S.; Braley, J.; Branch, K.; Broderick, K.; Carney, J.; Chevalier, J.; Choudhary, M. C.; Chowdhury, N.; Cordwell, T.; Daley, G.; Davidson, S.; Desjardins, M.; Donahue, L.; Drew, D.; Einkauf, K.; Elizabeth, S.; Elliman, A.; Etemad, B.; Fallon, J.; Fedirko, L.; Finn, K.; Flannery, J.; Forde, P.; Garcia-Broncano, P.; Gettings, E.; Golan, D.; Goodman, K.; Griffin, A.; Grimmel, S.; Grinke, K.; Hartana, C. A.; Healy, M.; Heller, H.; Henault, D.; Holland, G.; Jiang, C.; Jordan, H.; Kaplonek, P.; Karlson, E. W.; Karpell, M.; Kayitesi, C.; Lam, E. C.; LaValle, V.; Lefteri, K.; Lian, X.; Lichterfeld, M.; Lingwood, D.; Liu, H.; Liu, J.; Lopez, K.; Lu, Y.; Luthern, S.; Ly, N. L.; MacGowan, M.; Magispoc, K.; Marchewka, J.; Martino, B.; McNamara, R.; Michell, A.; Millstrom, I.; Miranda, N.; Nambu, C.; Nelson, S.; Noone, M.; Novack, L.; O'Callaghan, C.; Ommerborn, C.; Osborn, M.; Pacheco, L. C.; Phan, N.; Pillai, S.; Porto, F. A.; Rassadkina, Y.; Reissis, A.; Ruzicka, F.; Seiger, K.; Selleck, K.; Sessa, L.; Sharpe, A.; Sharr, C.; Shin, S.; Singh, N.; Slaughenhaupt, S.; Sheppard, K. S.; Sun, W.; Sun, X.; Suschana, E.; Talabi, O.; Ticheli, H.; Weiss, S. T.; Wilson, V.; Zhu, A. SARS-CoV-2 viral load is associated with increased disease severity and mortality. *Nat. Commun.* **2020**, *11*, No. 5493.
(12) Rao, K.; Verma, P.; Kumar, K.; Verma, M. K.; Siddiqui, A. H.; Singh, S.; Dhakar, J. S.; Kuru, C. I.; Sharma, P. K.; Soni, N. O.; Aryal, S. Review on Newly Identified Coronavirus and its Genomic Organization. *SSR Inst. Int. J. Life Sci.* **2020**, *6*, 2509−2519.
(13) Mujawar, M. A.; Gohel, H.; Bhardwaj, S. K.; Srinivasan, S.; Hickman, N.; Kaushik, A. Nano-enabled biosensing systems for intelligent healthcare: towards COVID-19 management. *Mater. Today Chem.* **2020**, *17*, 100306−100315.
(14) Lee, D.; Lee, J. Testing on the move: South Korea's rapid response to the COVID-19 pandemic. *Transp. Res. Interdiscip. Perspect.* **2020**, *5*, 100111−100120.
(15) Emery, S. L.; Erdman, D. D.; Bowen, M. D.; Newton, B. R.; Winchell, J. M.; Meyer, R. F.; Tong, S.; Cook, B. T.; Holloway, B. P.; McCaustland, K. A.; Rota, P. A.; Bankamp, B.; Lowe, L. E.; Ksiazek, T. G.; Bellini, W. J.; Anderson, L. J. Real-Time Reverse Transcription−Polymerase Chain Reaction Assay for SARS-associated Coronavirus. *Emerging Infect. Dis.* **2004**, *10*, 311−316.
(16) Mishra, S.; Kim, E. S.; Sharma, P. K.; Wang, Z. J.; Yang, S. H.; Kaushik, A. K.; Wang, C.; Li, Y.; Kim, N. Y. Tailored Biofunctionalized Biosensor for the Label-Free Sensing of Prostate-Specific Antigen. *ACS Appl. Bio Mater.* **2020**, *3*, 7821−7830.
(17) Wang, L.; Veselinovic, M.; Yang, L.; Geiss, B. J.; Dandy, D. S.; Chen, T. A sensitive DNA capacitive biosensor using interdigitated electrodes. *Biosens. Bioelectron.* **2017**, *87*, 646−653.
(18) Ravi, N.; Cortade, D. L.; Ng, E.; Wang, S. X. Diagnostics for SARS-CoV-2 detection: A comprehensive review of the FDA-EUA COVID-19 testing landscape. *Biosens. Bioelectron.* **2020**, *165*, 112454−112467.
(19) Sethuraman, N.; Jeremiah, S. S.; Ryo, A. Interpreting Diagnostic Tests for SARS-CoV-2. *J. Am. Med. Assoc.* **2020**, *323*, 2249−2251.
(20) Timmer, W. C.; Villalobos, J. M. The polymerase chain reaction. *J. Chem. Educ.* **1993**, *70*, 273−280.
(21) Whitesides, G. M. The origins and the future of microfluidics. *Nature* **2006**, *442*, 368−373.
(22) Drummond, T. G.; Hill, M. G.; Barton, J. K. Electrochemical DNA sensors. *Nat. Biotechnol.* **2003**, *21*, 1192−1199.
(23) Singhal, C.; Khanuja, M.; Chaudhary, N.; Pundir, C. S.; Narang, J. Detection of chikungunya virus DNA using two-dimensional MoS_2 nanosheets based disposable biosensor. *Sci. Rep.* **2018**, *8*, No. 7734.
(24) Sharma, P. K.; Dorlikar, S.; Rawat, P.; Malik, V.; Vats, N.; Sharma, M.; Rhyee, J. S.; Kaushik, A. K. Nanotechnology and Its Application: A Review. In *Nanotechnology in Cancer Management*; Elsevier, 2021; pp 1−33.
(25) Brasil, P.; Pereira, J. P.; Moreira, M. E.; Ribeiro Nogueira, R. M.; Damasceno, L.; Wakimoto, M.; Rabello, R. S.; Valderramos, S. G.; Halai, U.-A.; Salles, T. S.; Zin, A. A.; Horovitz, D.; Daltro, P.; Boechat, M.; Raja Gabaglia, C.; Carvalho de Sequeira, P.; Pilotto, J. H.; Medialdea-Carrera, R.; Cotrim da Cunha, D.; Abreu de Carvalho, L. M.; Pone, M.; Machado Siqueira, A.; Calvet, G. A.; Rodrigues Baião, A. E.; Neves, E. S.; Nassar de Carvalho, P. R.; Hasue, R. H.; Marschik, P. B.; Einspieler, C.; Janzen, C.; Cherry, J. D.; Bispo de Filippis, A. M.; Nielsen-Saines, K. Zika Virus Infection in Pregnant Women in Rio de Janeiro. *N. Engl. J. Med.* **2016**, *375*, 2321−2334.
(26) Kong, J.; Franklin, N. R.; Zhou, C.; Chapline, M. G.; Peng, S.; Cho, K.; Dai, H. Nanotube Molecular Wires as Chemical Sensors. *Science* **2000**, *287*, 622−625.
(27) Wang, J. Carbon-Nanotube Based Electrochemical Biosensors: A Review. *Electroanalysis* **2005**, *17*, 7−14.
(28) Layqah, L. A.; Eissa, S. An electrochemical immunosensor for the corona virus associated with the Middle East respiratory syndrome using an array of gold nanoparticle-modified carbon electrodes. *Microchim. Acta* **2019**, *186*, 1−10.
(29) Vermisoglou, E.; Panáček, D.; Jayaramulu, K.; Pykal, M.; Frébort, I.; Kolář, M.; Hajdúch, M.; Zbořil, R.; Otyepka, M. Human virus detection with graphene-based materials. *Biosens. Bioelectron.* **2020**, *166*, 112436−112457.
(30) Ali, Md. A.; Hu, C.; Jahan, S.; Yuan, B.; Saleh, M. S.; Ju, E.; Gao, S.-J.; Panat, R. Sensing of COVID-19 Antibodies in Seconds via

https://doi.org/10.1021/acssensors.1c01437
ACS Sens. 2021, 6, 3468−3476

Aerosol Jet Nanoprinted Reduced-Graphene-Oxide-virtue Coated 3D Electrodes. *Adv. Mater.* **2021**, *33*, 2006647−2006662.
(31) Kim, N. Y.; Adhikari, K.; Dhakal, R.; Chuluunbaata, Z.; Wang, C.; Kim, E. S. Rapid, Sensitive and Reusable Detection of Glucose by a Robust Radiofrequency Integrated Passive Device Biosensor Chip. *Sci. Rep.* **2015**, *5*, No. 7807.
(32) Hwang, C.; Park, N.; Kim, E. S.; Kim, M.; Kim, S. D.; Park, S.; Kim, N. Y.; Kim, J. H. Ultra-fast and recyclable DNA biosensor for point-of-care detection of SARS-CoV-2 (COVID-19). *Biosens. Bioelectron.* **2021**, *185*, 113177−113183.
(33) Kang, P.; Wang, M. C.; Nam, S. Bioelectronics with two-dimensional materials. *Microelectron. Eng.* **2016**, *161*, 18−35.
(34) Syama, S.; Mohanan, P. V. Comprehensive Application of Graphene: Emphasis on Biomedical Concerns. *Nano-Micro Lett.* **2019**, *11*, 6−36.
(35) Kim, E. S.; Liang, J. G.; Wang, C.; Cho, M. Y.; Oh, J. M.; Kim, N. Y. Inter-digital capacitors with aerosol-deposited high-K dielectric layer for highest capacitance value in capacitive super-sensing applications. *Sci. Rep.* **2019**, *9*, No. 680.
(36) Qiang, T.; Wang, C.; Kim, N. Y. Quantitative detection of glucose level based on radiofrequency patch biosensor combined with volume-fixed structures. *Biosens. Bioelectron.* **2017**, *98*, 357−363.
(37) Feng, J.; Guo, Z. Wettability of graphene: from influencing factors and reversible conversions to potential applications. *Nanoscale Horiz.* **2019**, *4*, 526−530.
(38) Flynn, S. P.; McKenna, M.; Monaghan, R.; Kelleher, S. M.; Daniels, S.; MacCormac, A. Aqua-Art: A Demonstration of Hydrophilic and Hydrophobic Surfaces Fabricated by Plasma Enhanced Chemical Vapor Deposition. *J. Chem. Educ.* **2017**, *94*, 221−225.
(39) Bhardwaj, S. K.; Yadav, P.; Ghosh, S.; Basu, T.; Mahapatro, A. K. Biosensing Test-Bed Using Electrochemically Deposited Reduced Graphene Oxide. *ACS Appl. Mater. Interfaces* **2016**, *8*, 24350−24360.
(40) Trilling, A. K.; Beekwilder, J.; Zuilhof, H. Antibody orientation on biosensor surfaces: a minireview. *Analyst* **2013**, *138*, 1619−1627.
(41) Ates, B.; Koytepe, S.; Ulu, A.; Gurses, C.; Thakur, V. K. Chemistry, Structures, and Advanced Applications of Nanocomposites from Biorenewable Resources. *Chem. Rev.* **2020**, *120*, 9304−9362.

https://doi.org/10.1021/acssensors.1c01437
ACS Sens. 2021, 6, 3468−3476